Electronic supplementary information (ESI)

Details of the photophysical measurements:

Luminescence spectra.

Luminescence spectra of compounds **2** and **3** at 298 and 77 K (Fig. 1–4), of **4** at 77 K (Fig. 6), and of **7**–**9** at 298 and 77 K (Fig. 7–11 and Fig. 5 in the manuscript) were measured with a Hitachi F4500 luminescence spectrometer. A contour plot of **4** at 77 K (Fig. 5) is also shown in order to confirm that a strong single emission from a ^{3}MLCT state is present at this temperature, disappearing already above 122 K (Fig. 12). The concentrations for room temperature measurements were:

Sample **2**: 2.3 mg / 2.0 ml.
Sample **3**: 2.2 mg / 2.0 ml.
Sample **7**: 2.1 mg / 2.0 ml.
Sample **8**: 2.1 mg / 2.0 ml.
Sample **9**: 2.0 mg / 2.0 ml.

The solvent is acetonitrile (CH_3CN), degassed spectrograde quality. The spectra were recorded with the following parameters: Vpmt: 900 V, excitation range: 200 – 800 nm, excitation bandwidth: 5 nm, emission range: 300 – 800 nm, emission bandwidth: 5 nm, scan speed: 240 nm/ min. The integration time was adjusted automatically by the software to match the scan speed. These spectra are not compensated for the instrument response function. Over this range the instrument response is not expected to show strong variation.

The concentrations for room temperature measurements have been chosen in order to obtain “good” signal/noise ratios. All these concentrations fulfil the condition A<1, where A<1 can generally be used. However, it is completely clear that for quantum efficiency measurements these concentrations are too high. It is clearly stated below that the concentration of adjusted solutions was tuned to make the absorptions for samples **2** – **4** and **7** – **9** in OD <0.1. Furthermore, it is also emphasized below that the wavelength dependence of the quantum efficiency has been corrected and lamp corrections were made. Of course, we have checked in all cases that the Contour plots and hence also the emission and excitation spectra remain the same, when diluting the samples.

Nevertheless, all spectra have been repeated with a Varian Caray Eclipse Spectrometer, allowing a “good” correction for the wavelength response of the excitation system (lamp + monochromator). Diluted solutions of the samples, with A<0.1 in the whole spectral range have been used. As a matter of fact all Contour plots and hence also the emission and excitation spectra are identical to the plots and spectra obtained with the different instrument! Obviously, also with regard to the former, more concentrated measurements the conditions have been chosen “good enough” in order to guarantee that the results are right.

The lowest energy MLCT (Os→bpy) absorption band occurs at 475 nm in the case of **9**. Fig. 5 of the manuscript clearly shows that excitation of **9** at 467 nm leads to the typical emission at 595 nm. This means that a good practice to record emission spectra requires excitation of the sample near the maximum of the lowest-energy absorption band. However, Fig. 5 also shows a second excitation maximum at 370 nm being close to the maximum of the MLCT (Ru→bpy) absorption band at 362 nm. Furthermore, in Fig. 5 a third excitation maximum at 300 nm appears, being close to the maximum of the metal-centred (MC) d→d transition at 317 nm. At this point it is important to note that all three excitation maxima lead to the same emission at 595 nm, clearly indicating that the excitation wavelength should not be overestimated, since the same emissive state is populated. Even more important is the fact that all three excitation maxima are close to clearly identified absorption maxima. In this case, the shape of the excitation spectrum is the replica of the absorption spectrum of the emitting species.

In the case of **7** no lowest energy MLCT absorption band maximum can be appreciated from Fig. 15 below, ESI. Therefore, the lowest energy absorption band maximum is the metal-centred (MC) d→d transition at 318 nm. Again excitation is performed close to this maximum, namely at 325 nm (see Fig. 7, ESI). Also in this case a second excitation maximum appears at 275 nm close to the intraligand (IL) transition maximum at 270 nm in the absorption spectrum. Both excitation maxima lead to the same emission at 385 nm. As before, the absorption and excitation maxima nearly coincide and hence also in this case the shape of the excitation spectrum is the replica of the absorption spectrum.

Due to the similarity of the molecules, the photophysical behaviour of **8** is completely analogous to **7**: excitation close to the intraligand (IL) transition maximum at 270 nm in the absorption spectrum of **8** leads to the only observable emission band maximum at 400 nm (see Fig. 9, ESI). Excitations close to the absorption band maximum of the MC d→d transition at 318 nm and close to the lowest energy absorption band maximum of the MLCT transition at 343 nm lead to the same emission at 400 nm. Again all three absorption band maxima of **8** are close to the corresponding excitation band maxima observed in Fig. 9, ESI. This means that also in the case of **8** the excitation spectrum is the replica of the absorption spectrum.

4 shows no emission at all at ambient temperature. The unusual behaviour of **2** and **3** must have a different explanation due to the special properties of these compounds (*vide infra*). Regarding the emission spectra, in all cases careful Contour plots have been measured in order to locate the emissions. They have been repeated with $A<0.1$, a correction for the wavelength response of the excitation system and with a different instrument, showing the same results. In the case of **2** the lowest energy absorption band maximum of the MLCT transition is observed at 377 nm. As a matter of fact, the Contour plot of **2** unequivocally reveals that using an excitation wavelength of 377 nm leads to no emission at all. Fig. 1, ESI, displays the only observable emission for **2**, where the excitation maximum occurs at 530 nm. In the case of **3** the lowest energy absorption band maximum of the MLCT transition is observed at 356 nm. The Contour plot of **3** shows that for an excitation wavelength of 356 nm the resulting emission is only very weak, where this can also be seen in Fig. 3, ESI. However, also in this case the different excitation wavelengths in Fig. 3, showing a maximum at 465 nm, lead to the same emission at 600 nm. The excitations of **2** and **3** within the red tails of the MLCT absorption bands are unusual. A possible explanation is given below.

All excitation spectra have been recorded using the wavelength of the emission maximum as the emission wavelength. They have been repeated with a different instrument allowing a correction for the wavelength response of the excitation system (lamp + monochromator) and with A<0.1 in the whole spectral range, leading to the same results (only the signal/noise ratio is worse compared with the more concentrated samples!). It has been described in the section above that for the complexes **7** – **9** the absorption band maxima nearly coincide with the excitation maxima. In these cases the shape of the excitation spectrum is indeed the replica of the absorption spectrum of the emitting species.

However, **4** is a limit case, showing that exceptions could exist. The absorption spectrum of **4** is shown in Fig. 14, ESI, but in this case the excitation spectrum can not be the replica of the absorption spectrum. **4** is non-emissive at ambient temperature and its “excitation spectrum” would be a “zero line”. Obviously, there must be a physical effect that dramatically influences the excitation spectrum, but not the absorption spectrum. This effect is the very rapid population of the metal-centred (MC) d→d state, leading to an ultrafast radiationless decay of the excited states of **4**. It is clearly stated in the manuscript that also in **2** and **3** this MC d→d state is readily populated. Analogous to **4** most of the incoming energy is immediately released *via* non-radiative decay of the MC d→d state also in **2** and **3**. Obviously, only the red tails of the manifold of MLCT absorption bands lead to a residual emission. They are low in energy and therefore the population of the MC d→d states could be partly inhibited, where also “steric pressure” could be important in line with the discussion in the manuscript. As a consequence, the excitation spectra of **2** and **3** should be regarded as intermediate cases between the “zero line” of **4** and “full” excitation spectra.

The concentrations of the samples for measurements at 77 K were:
Sample **2**: 3.1 mg / 2.0 ml.
Sample **3**: 4.2 mg / 2.0 ml.
Sample **4**: 3.5 mg / 2.0 ml.
Sample **7**: 3.8 mg / 2.0 ml.
Sample **8**: 2.6 mg / 2.0 ml.
Sample **9**: 2.0 mg / 2.0 ml.

The solvent for **2–4** is a 4:1:2 (v/v, degassed spectrograde quality) EtOH/MeOH/CH_3CN mixture forming a cryogenic glass. In order to improve the emissions for **7–9** a 10:1:5 (v/v, degassed spectrograde quality) EtOH/glycerol/CH_3CN mixture was used, forming better cryogenic glasses in these cases. However, the use of EtOH/MeOH (see ref. 12*a*) or propionitrile/butyronitrile (see ref. 27) glasses was not possible due to the complete insolubility of **2–4** and **7–9** in these solvent mixtures. Since at 77 K **2–4** and **7–9** are extremely intense emitters, the pmt voltage in the spectrometer was reduced to 700 V.

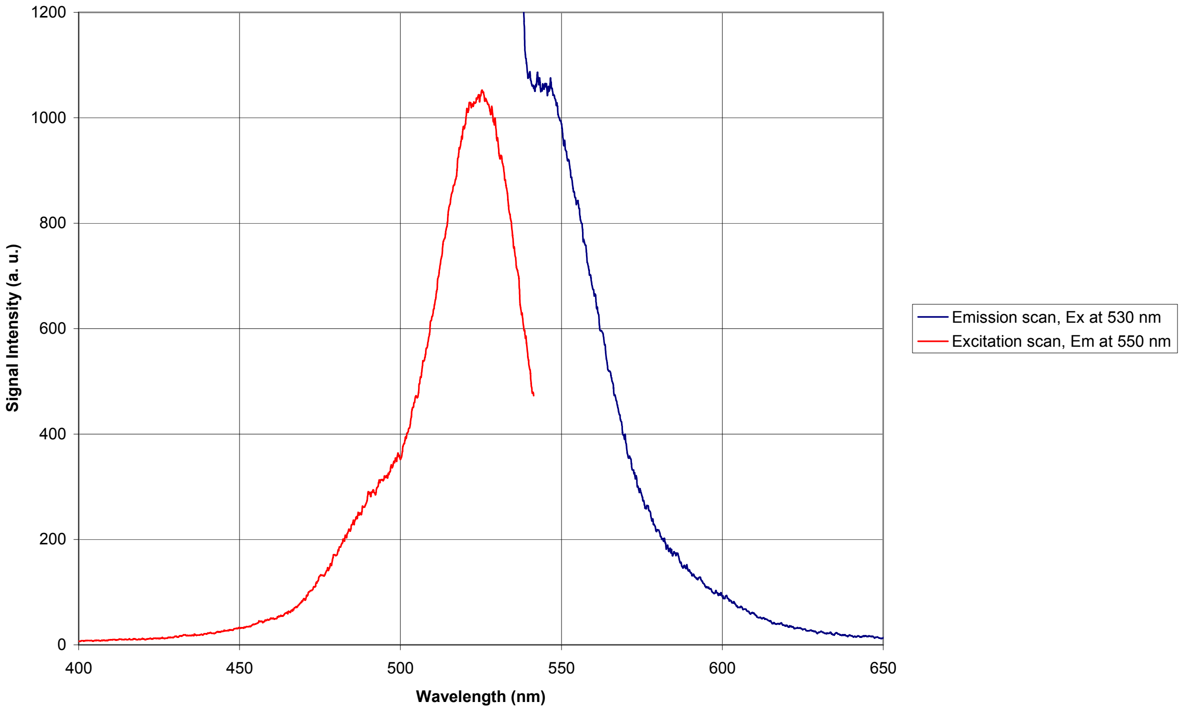

Fig. 1 Excitation and emission spectra of **2** in degassed spectrograde CH_3CN at 298 K.

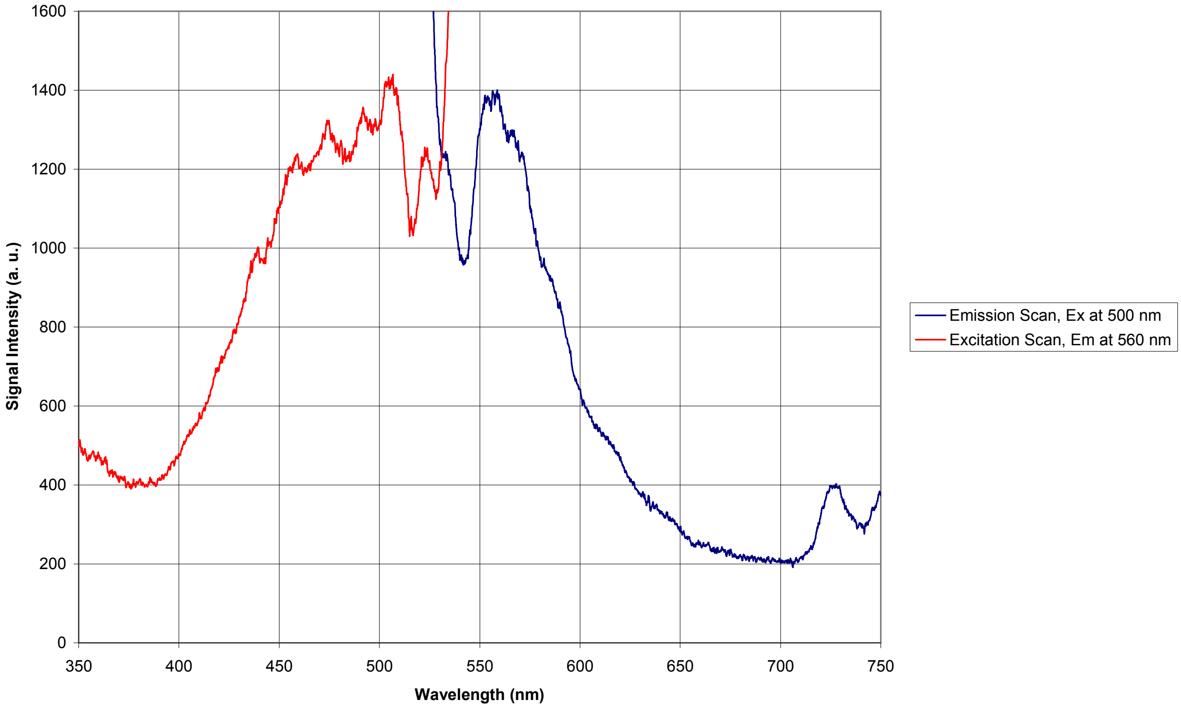

Fig. 2 Excitation and emission spectra of **2** in a 4:1:2 (v/v, degassed spectrograde quality) $EtOH/MeOH/CH_3CN$ mixture at 77 K.

S5

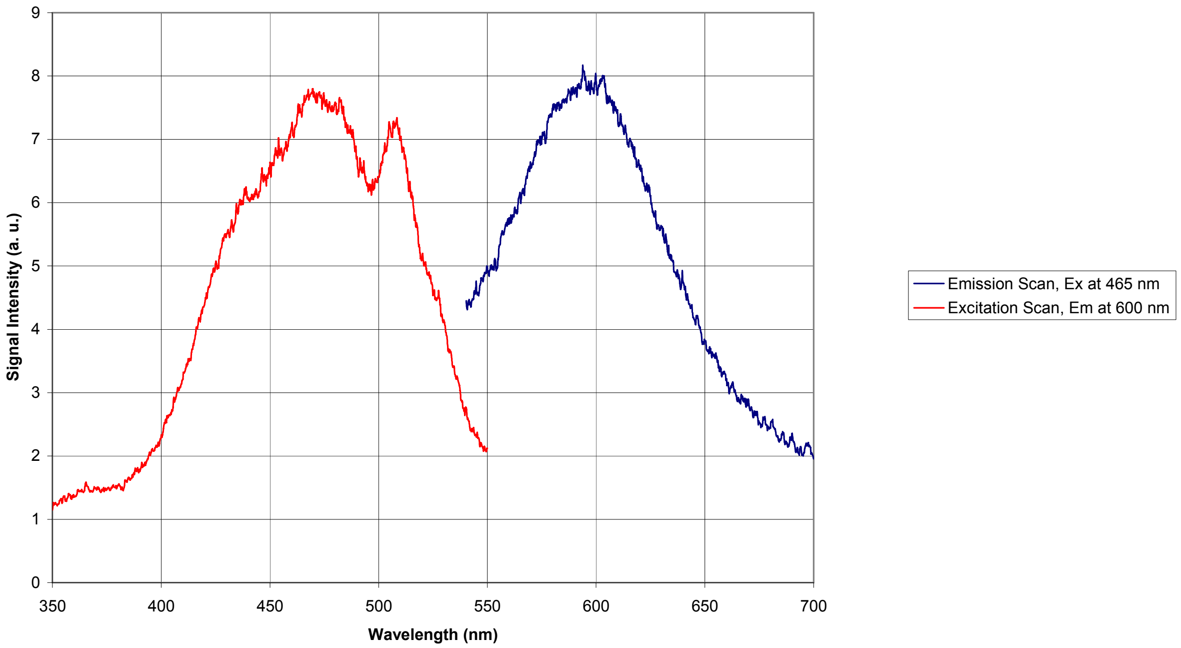

Fig. 3 Excitation and emission spectra of **3** in degassed spectrograde CH_3CN at 298 K.

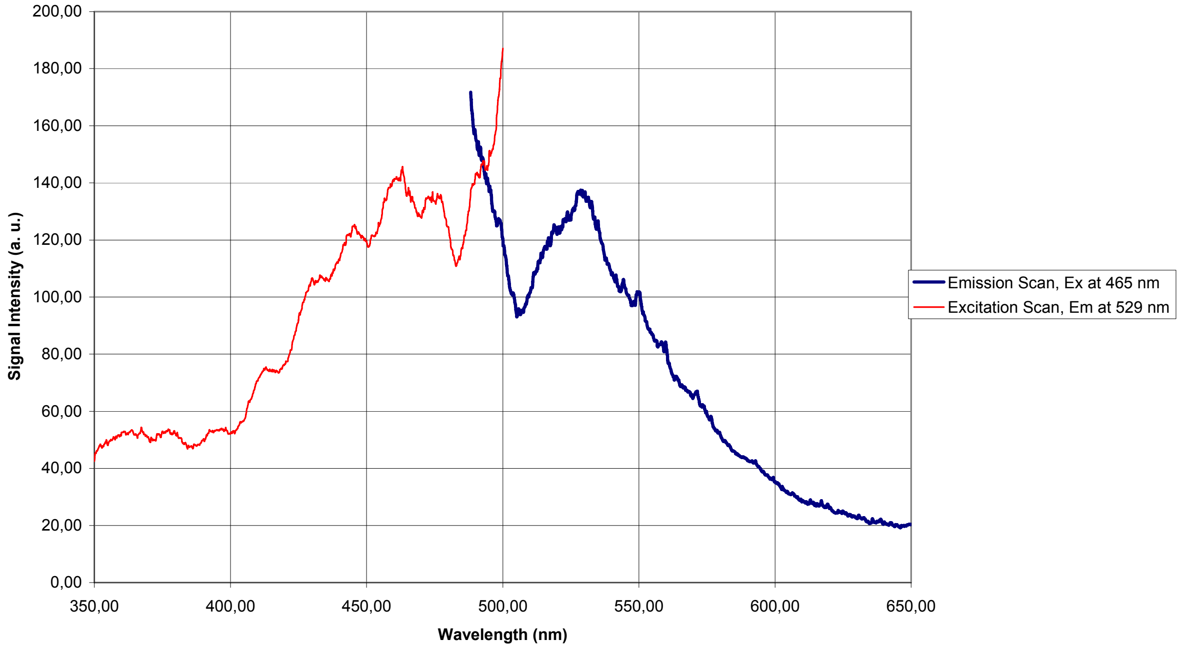

Fig. 4 Excitation and emission spectra of **3** in a 4:1:2 (v/v, degassed spectrograde quality) EtOH/MeOH/CH_3CN mixture at 77 K.

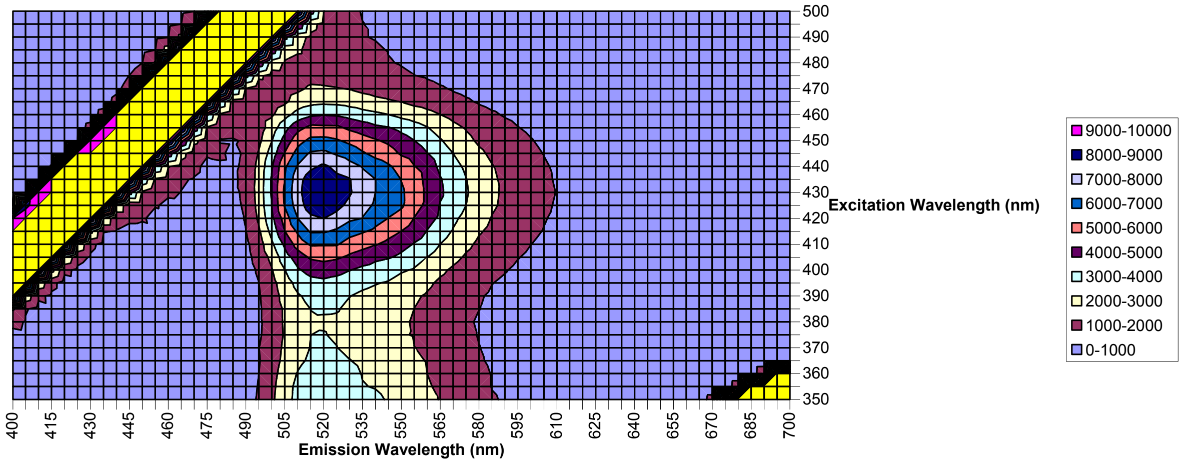

Fig. 5 Contour plot of the combined visible excitation and luminescence spectra of **4** in a 4:1:2 (v/v, degassed spectrograde quality) EtOH/MeOH/CH_3CN mixture at 77 K.

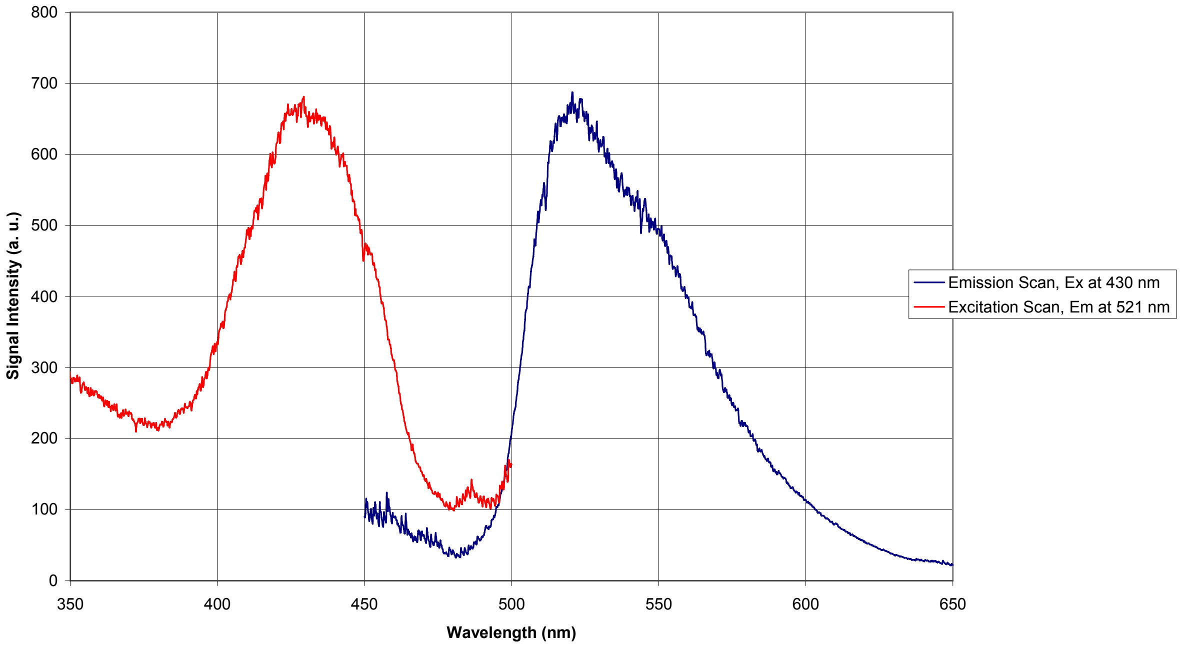

Fig. 6 Excitation and emission spectra of **4** in a 4:1:2 (v/v, degassed spectrograde quality) EtOH/MeOH/CH_3CN mixture at 77 K.

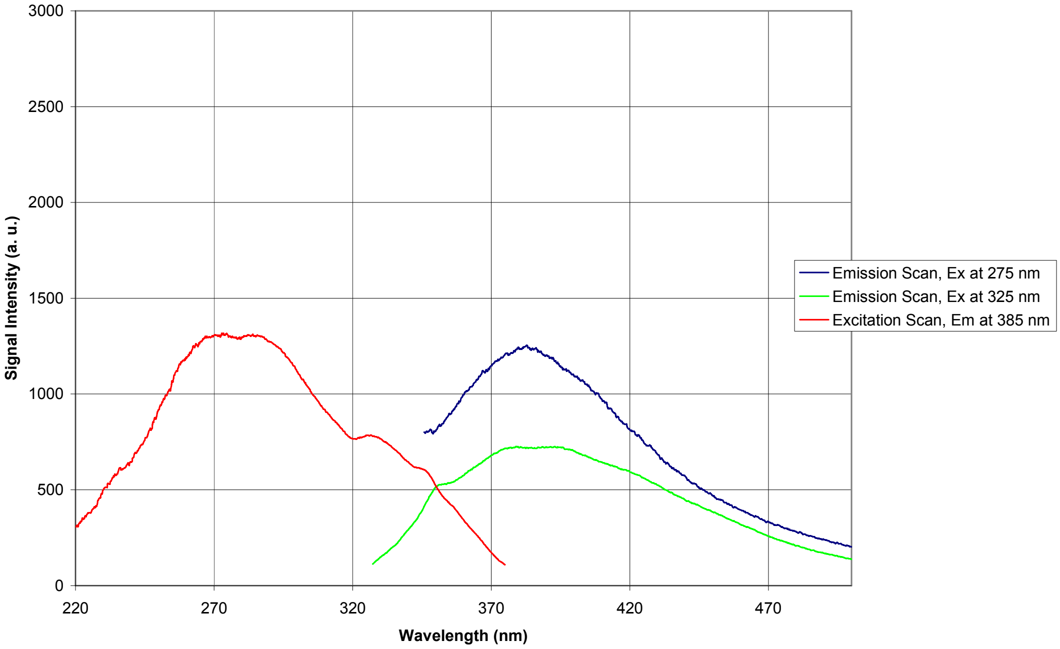

Fig. 7 Excitation and emission spectra of **7** in degassed spectrograde CH_3CN at 298 K.

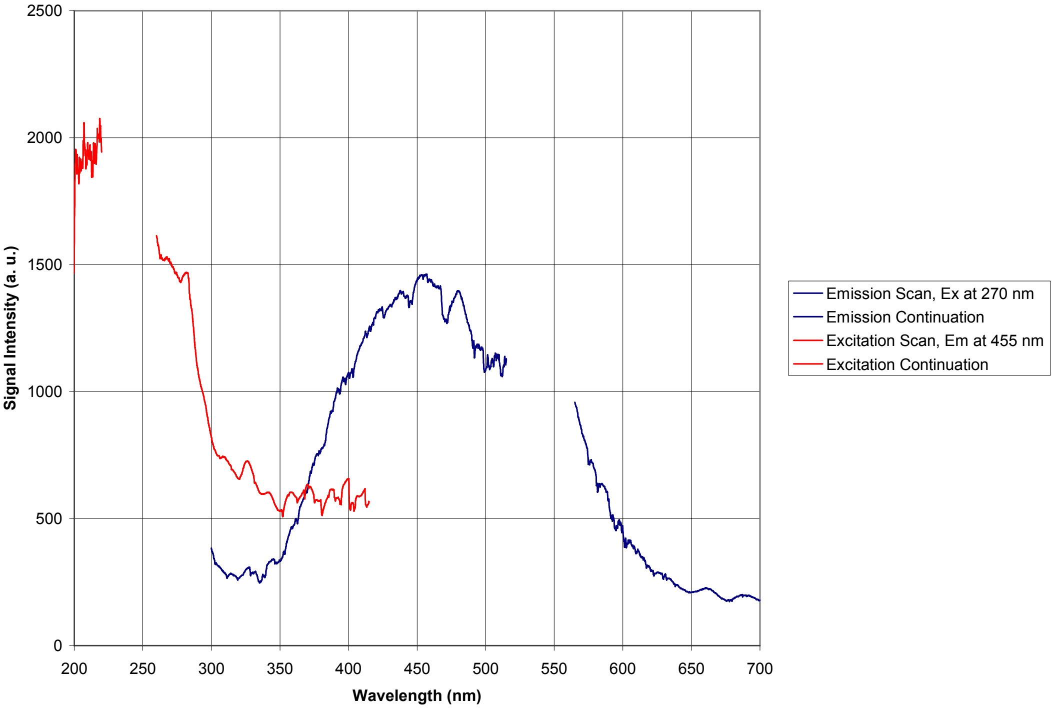

Fig. 8 Excitation and emission spectra of **7** in a 10:1:5 (v/v, degassed spectrograde quality) $EtOH$/glycerol/CH_3CN mixture at 77 K, regions with Rayleigh scattering *via* second order grating of the spectrometer removed.

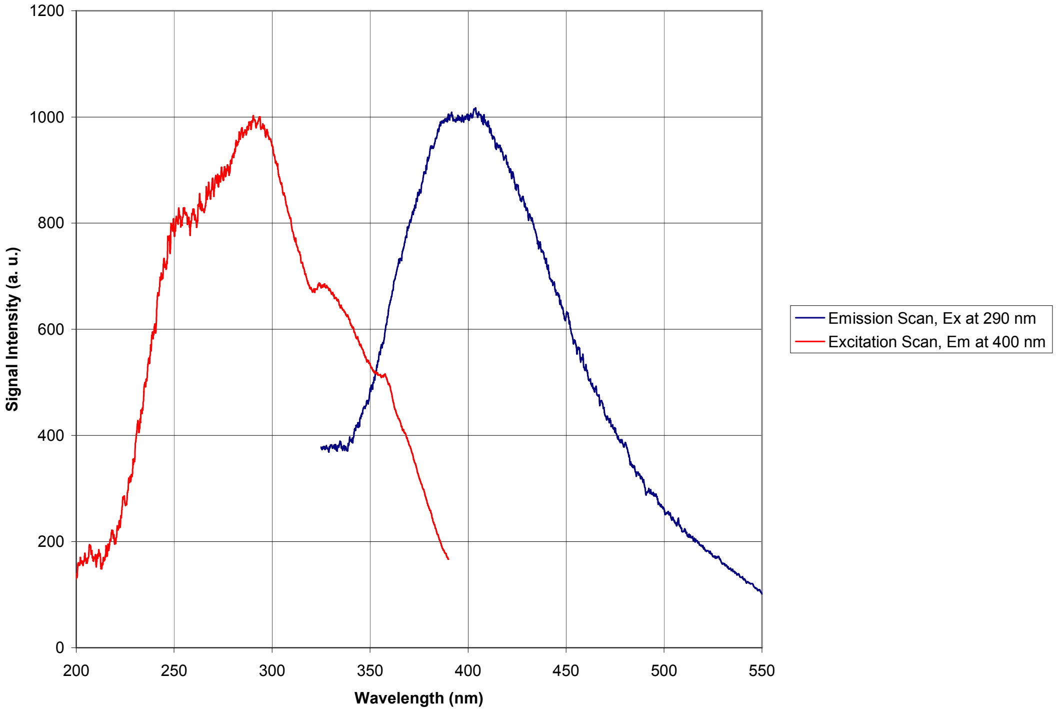

Fig. 9 Excitation and emission spectra of **8** in degassed spectrograde CH_3CN at 298 K.

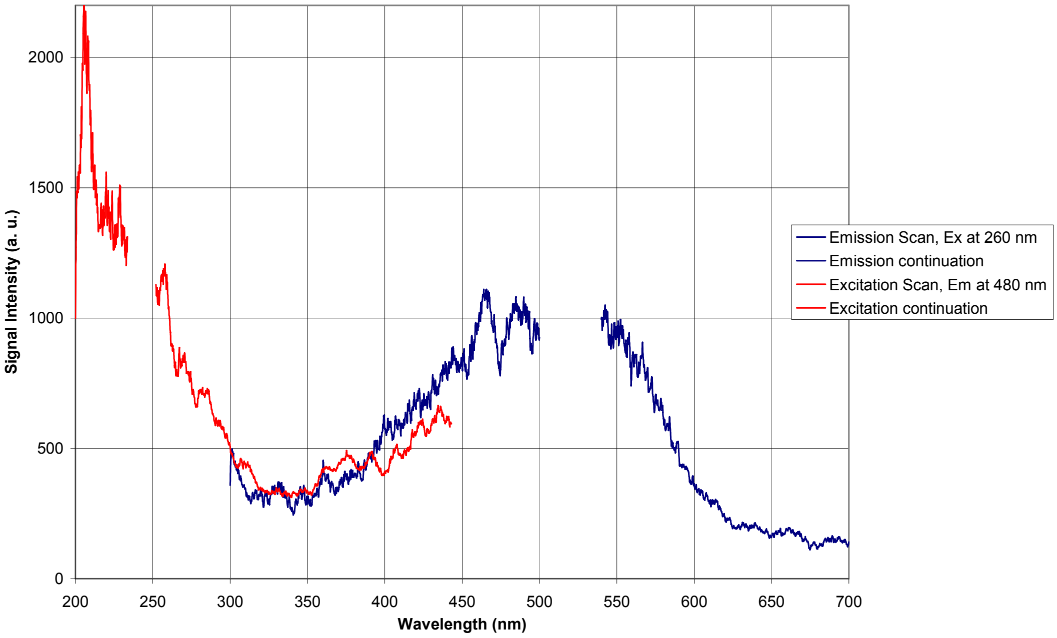

Fig. 10 Excitation and emission spectra of **8** in a 10:1:5 (v/v, degassed spectrograde quality) EtOH/glycerol/CH_3CN mixture at 77K, regions with Rayleigh scattering *via* second order grating of the spectrometer removed.

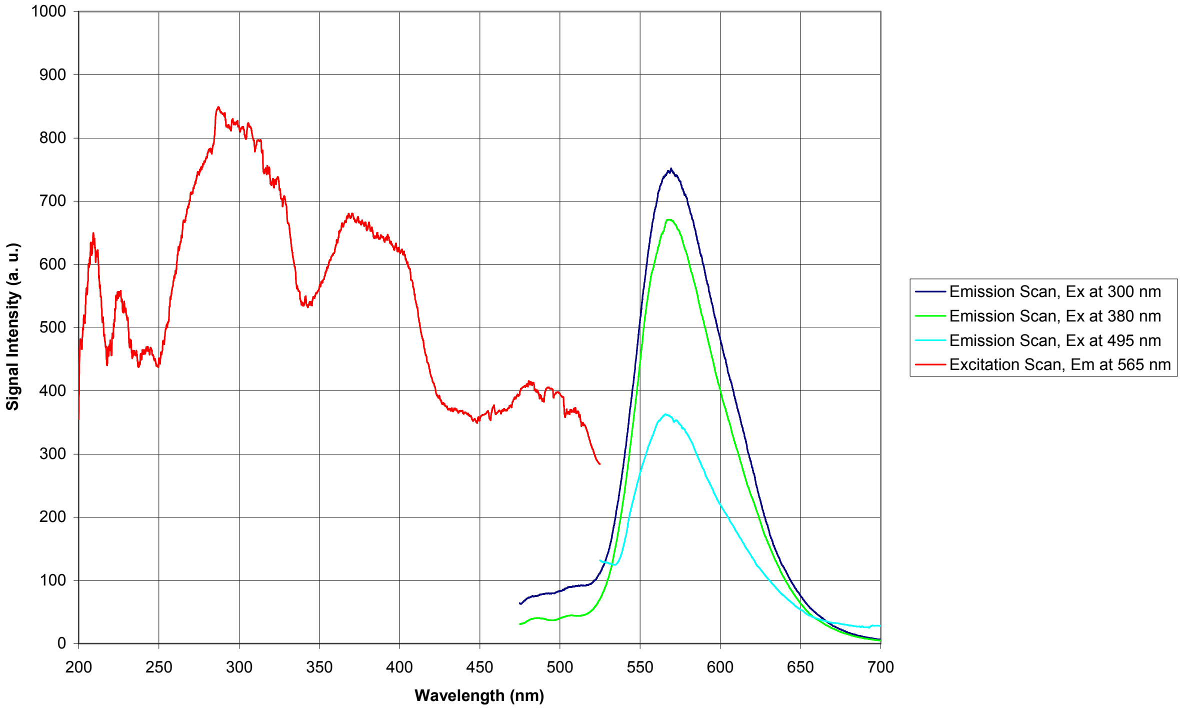

Fig. 11 Excitation and emission spectra of **9** in a 10:1:5 (v/v, degassed spectrograde quality) EtOH/glycerol/CH_3CN mixture at 77 K.

Lifetime.

The luminescence lifetime measurements of **2**–**4** and **7**–**9** are summarized in Table 1. Fig. 12 and 13 show plots of ln τ vs. $1000/T$ (K^{-1}) for **4** and **9**. Lifetimes were measured with a nanosecond laser/OPO system (Continuum Surelite). The luminescence radiation is collected and directed into a monochromator (Spex 270M) and detected with a photo multiplier (Hamamatsu R928). The electric signal from the pmt was digitized and averaged over 250 shots with a digital sampling oscilloscope (LeCroy 9350A). For each measurement a background signal was also recorded and subtracted from the signal.

The samples were measured in a cell with optical path length 1 cm. The concentrations and solvents for the measurements at room temperature and 77 K were the same as given above. For variable temperature lifetime measurements between 77 and 298 K the samples for the measurements at 77 K were used as given above. In the cases **3**, **4**, and **7**–**9** all lifetimes can be fitted by single exponential decay functions independent of excitation wavelength in the whole temperature range 77–298 K. However, in the case of **2** the measurements of the lifetimes indicate the presence of a long and a short component.

For the lifetimes of **2** (short component, see Table 1 below) and the energy transfer experiments of **9** a picosecond laser setup was used. Pulses with a duration of ~20 ps and wavelength 532 nm were obtained from a frequency doubled Ekspla PL2143B mode locked Nd:YAG laser and directed into the sample cell. The fluorescence from the sample was collected perpendicular to the laser beam with a 100 mm focal length lens. Directly scattered light was removed with a Schott OG570 colored glass filter. The remaining fluorescent radiation was detected with an ET2030A amplified silicon photo diode (Electro Optics Technology Inc.) with a bandwidth of 1.2 GHz and recorded with a 1 GHz bandwidth digital oscilloscope, Tektronix 680C. The response time of the detection system is < 500 ps.

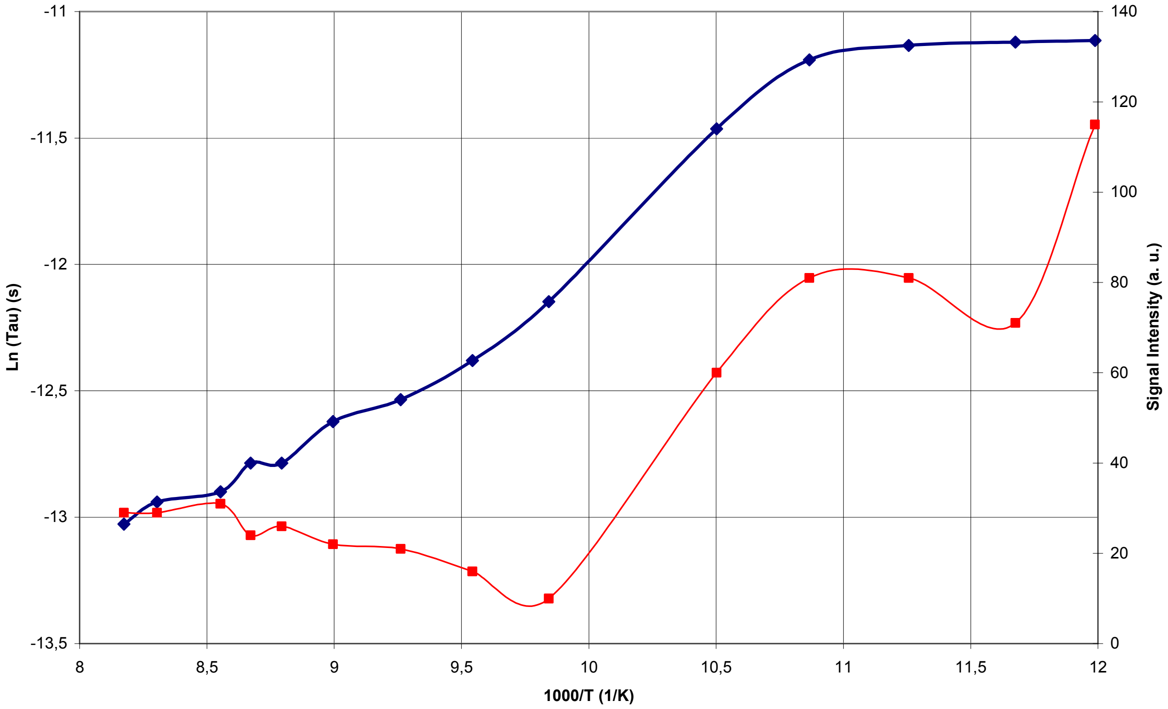

Fig. 12 Temperature dependence of the luminescence lifetime and the signal intensity of **4** in a 4:1:2 (v/v, degassed spectrograde quality) EtOH/MeOH/CH$_3$CN mixture.

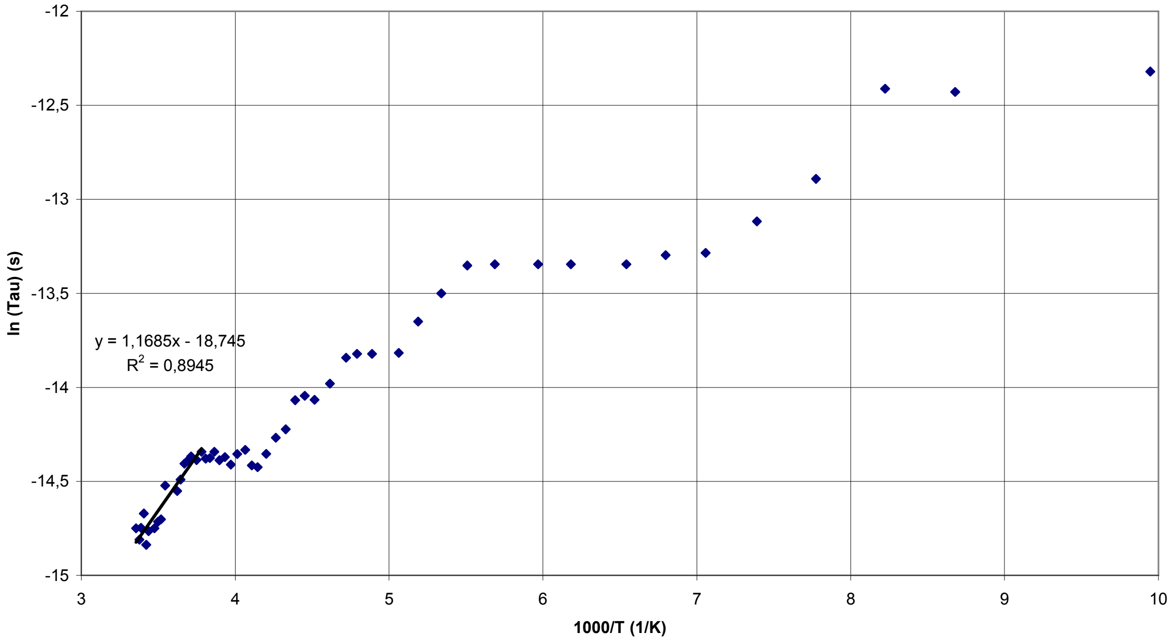

Fig. 13 Arrhenius plot of **9** in a 10:1:5 (v/v, degassed spectrograde quality) EtOH/glycerol/CH$_3$CN mixture.

The strong temperature dependence of the luminescent lifetimes in Fig. 12 and 13 clearly indicates that these emissions stem from ^{3}MLCT states (see ref. 12*a* and 27). Fig. 12 reveals that the luminescence of **4** completely disappears above 122 K. Therefore, only Fig. 13 shows the steep linear behaviour in the liquid range characteristic of the ^{3}MLCT → d→d crossover. A kinetic analysis of the dynamics of the ^{3}MLCT → d→d transition shows that the rate equation for RuP_2N_4 phosphine complexes in liquid solution has the Arrhenius-type form k' (experimentally observed rate constant) = $A \exp(-E_a/kT)$.[12a] The solid straight line in Fig. 13 is the best fit of the measured lifetimes in this temperature range and its equation is y = 1.1685 x – 18.745. From this equation the parameters E_a, k', and A were calculated. The corresponding parameters for **2** and **3** have been obtained in an analogous way (see Table 1).

Several careful tests have been carried out showing that the luminescent lifetimes of **2–4** and **7–9** are not obscured by trace impurities:

1) The temperature dependence of the luminescent lifetimes of **2–4** and **7–9** has been investigated within the temperature range 77–298 K. Single exponential decay functions have been used for all fitted lifetimes.
2) The lifetimes at 77 K are in line with other RuP_2N_4 complexes.[12a]
3) The temperature dependent lifetime-variations showing glass transitions are typical (see Fig. 13 and ref. 27).
4) For all photophysical measurements carefully purified crystals were used and dissolved in the corresponding degassed spectrograde quality solvents.

Absorption.

Absorption spectra were recorded for samples **2–4** and **7–9** using a Perkin and Elmer Lambda 900 photo spectrometer. A cell with optical path length 1 cm was used.

The concentration of adjusted solutions was tuned to make the absorptions for samples **2–4** and **7–9** in OD <0.1. The OD values for Rhodamine 6G and quinine sulfate dihydrate were also <0.1. The accurate absorption values are used in the quantum yield measurements. For higher accuracy these measurements were corrected for the losses (mostly by reflection) of a cell only containing acetonitrile and no sample.

For the quantum efficiency measurements of Rhodamine 6G and quinine sulfate dihydrate grey filters were used in the excitation beam. The OD of the filter for Rhodamine 6G was measured to be 2.160 and for quinine sulfate dihydrate 1.360.

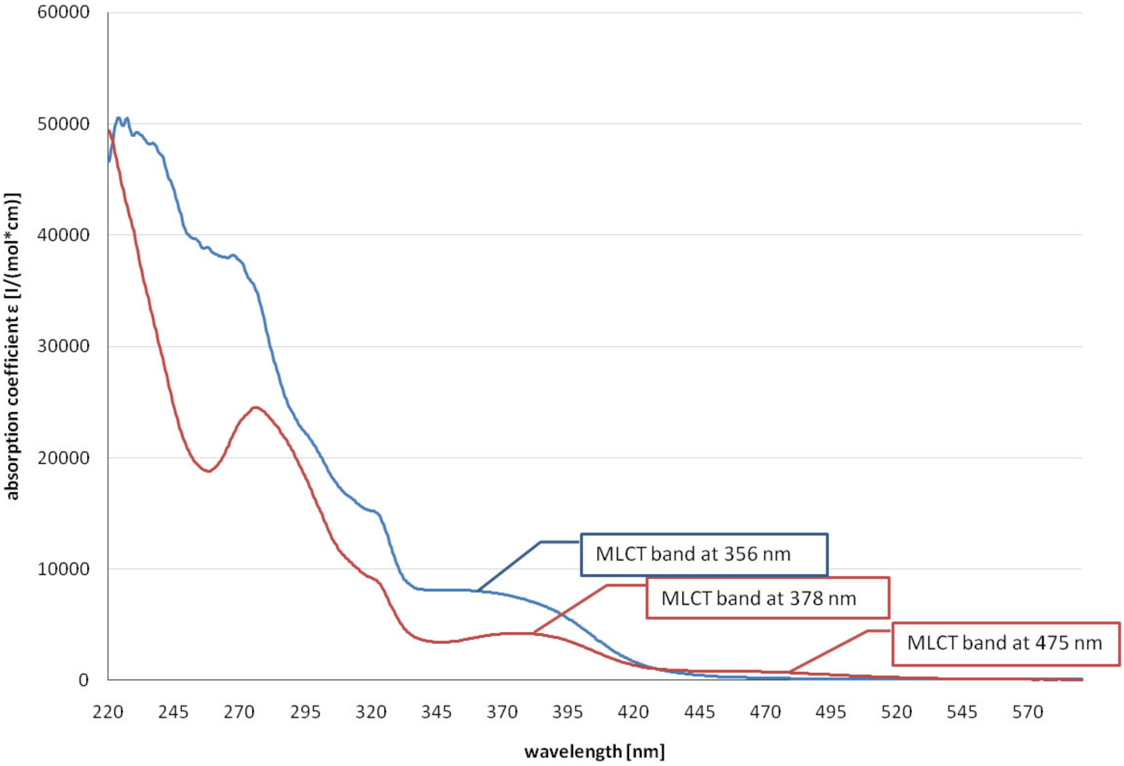

Fig. 14 UV-vis absorption spectra of **3** (blue) and **4** (red) in CH_3CN at ambient temperature, evidencing clearly the MLCT bands. The corresponding spectrum of **2** is nearly identical to **3** and has been omitted for clarity.

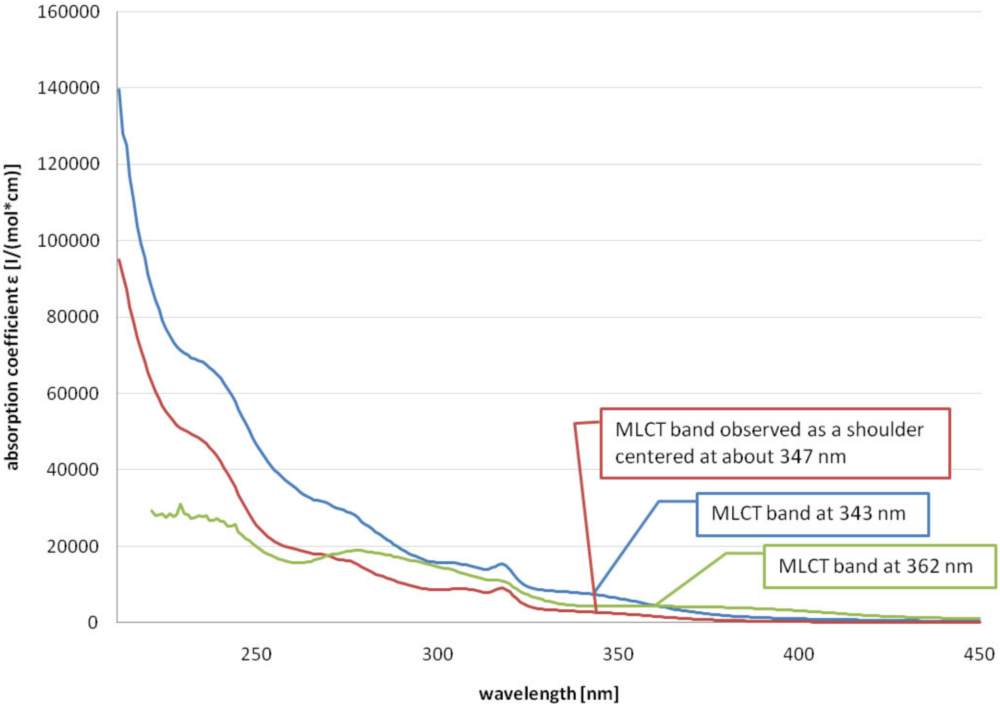

Fig. 15 UV-vis absorption spectra of **7** (red), **8** (blue), and **9** (green) in CH_3CN at ambient temperature, evidencing clearly the MLCT bands. In the case of **9** the MLCT (Os→bpy) absorption extending to ca. 600 nm is not shown due to its low intensity.

Comparison between absorption and excitation spectra.

The emission quantum yields of compounds **2**, **3**, and **7** – **9** are very low (see Table 1). Compound **3** shows the smallest ϕ_r of $2.07\cdot10^{-4}$, where the excitation occurs between 350 and 550 nm at 298 K (see Fig. 3). A comparison with the absorption spectrum of the same compound (see Fig. 14) unequivocally reveals that the observed emission stems from the MLCT absorption. However, it is well-known that in heterodimetallic complexes like **3** orbital splitting leads to further stabilized MLCT excited states (see ref. 30 of the manuscript). From ϕ_r of **3** it is clear that the emission/absorption and hence also the excitation/absorption ratio is nearly 1:5000! In view of the manifold of MLCT excited states in **3** it is not clear which state dominates the emission, where of course all states are involved in the absorption. Therefore, it is more appropriate to show the excitation and emission spectra and not the absorption and emission spectra in this case. Regarding the shapes one should be aware that the excitation spectrum is only a very tiny part of the absorption spectrum. The absorption spectra of **2** and **7** – **9** can be compared in the same way with their corresponding excitation spectra. The excitation and emission band maxima for **2–4** and **7–9** are collected in Table 2.

Quantum efficiency.

The quantum efficiency of Rhodamine 6G is 0.95:

C. V. Bindhu, S. S. Harilal, V. P. N. Nampoori and C. P. G. Vallabhan, *Mod. Phys. Lett. B*, 1999, **13**, 563–576.

M. Fischer and J. Georges, *Chem. Phys. Lett.*, 1996, **260**, 115–118.

The quantum efficiency of quinine sulfate dihydrate is 0.51:

L. S. Rohwer and J. E. Martin, *J. Lumin.*, 2005, **115**, 77–90.

In the cases **2**, **3** and **9** Rhodamine 6G was chosen as the standard, because its fluorescence spectrum has a good overlap with the luminescence of the samples investigated, thus reducing possible instrument errors. For the same reasons quinine sulfate dihydrate was used for **7** and **8**. The wavelength dependence of the transmission of monochromators was taken into account. Like the absorptions of **2**, **3** and **7–9**, the absorptions of Rhodamine 6G and quinine sulfate dihydrate are more to the blue compared with $[Os(bpy)_3]^{2+}$ or $[Ru(bpy)_3]^{2+}$. It is well-known that the π acidity of phosphine ligands destabilizes the lowest MLCT state and this shift toward higher energies is typical for $Os(phosphine)_2(bpy)_2$ or $Ru(phosphine)_2(bpy)_2$ moieties (see ref. 4*b* and 12*a*). However, the quantum yield for $[Ru(bpy)_3]^{2+}$ was measured as a control:

the quantum efficiency of $[Ru(bpy)_3]^{2+}$ is 0.062 in CH_3CN (see ref. 13).

The major instrument error in the luminescence spectrometer is due to the wavelength dependence of the quantum efficiency of the photo multiplier, in this case Hamamatsu R928.

This function is fitted in the range between 300 and 800 nm. On a linear scale the quantum efficiency drops non-linear, so an exponential fit works:
$\mathrm{QE}(\lambda) = -5.26 + 100.76\, e^{-\lambda/316.17}$.

Since right angle viewing is used, the solutions of **2**, **3** and **7–9** used for the luminescence spectra at room temperature have been further diluted by a factor 1:10. Furthermore, lamp corrections were made.

The emission was fitted to a double Gaussian and the area was computed this way. Especially toward the excitation wavelength this fit of the experimental spectrum can be necessary. However, a numerical integral leads to the same result.

The curves were integrated over the corresponding peak ranges for **2**, **3** and **7–9** leading to the emission quantum yields (ϕ_r) given in Table 1.

Summary of the photophysical parameters.

Table 1 Photophysical parameters[a] for $[Ru(bpy)_2(dppcb)MCl_2](PF_6)_2$ (M = Pt, **2**; Pd, **3**; Ni, **4**), $[Ru(bpy)(CH_3CN)_2(dppcb)MCl_2](SbF_6)_2$ (M = Pt, **7**; Pd, **8**), and $[Ru(bpy)(CH_3CN)_2(dppcb)Os(bpy)_2](PF_6)_4$ (**9**)

Compound	τ^b 298 K, ns	τ 77 K, μs	ϕ_r^b 298 K	E_a cm^{-1}	k'^e 298 K, s^{-1}	A s^{-1}
2	299(6), 3.5(5)	4.4(3),^{c} 6.4(5) ns^c	0.0060	408^c	$3.40\cdot10^6$	$2.44\cdot10^7$
3	261(10)	12.2(1)^c	$2.07\cdot10^{-4}$	297^c	$4.93\cdot10^6$	$2.07\cdot10^7$
4		14.80(4)^c				
7	17.0(2)	5.5(6)^d	0.014			
8	12.10(8)	4.5(2)^d	0.057			
9	297(4)	4.3(1)^d	0.022	812^d	$2.74\cdot10^6$	$1.38\cdot10^8$

[a] The excitation/emission wavelengths (nm) are: **2**. Long component: 520/600 (298 K), 480/580 (77 K); short component: 500/575 (298 K), 475/560 (77 K). **3**. 465/600 (298 K), 430/525 (77 K). **4**. 430/520 (77 K). **7**. 350/420 (298 K), 350/450 (77 K). **8**. 350/420 (298 K), 350/450 (77 K). **9**. 370/595 (298 K), 380/565 (77 K). [b] In degassed spectrograde CH_3CN. [c] In a 4:1:2 (v/v, degassed spectrograde quality) $EtOH/MeOH/CH_3CN$ mixture. [d] In a 10:1:5 (v/v, degassed spectrograde quality) $EtOH$/glycerol/CH_3CN mixture. [e] These values indicate an enhanced rate for the ^{3}MLCT → d→d transition compared, for example, to that of $[Ru(bpy)_3]^{2+}$, where $k'(298\text{ K}) = 1.7\cdot10^6\ \mathrm{s}^{-1}$.[12a]

Table 2 Excitation and emission band maxima for $[Ru(bpy)_2(dppcb)MCl_2](PF_6)_2$ (M = Pt, **2**; Pd, **3**; Ni, **4**), $[Ru(bpy)(CH_3CN)_2(dppcb)MCl_2](SbF_6)_2$ (M = Pt, **7**; Pd, **8**), and $[Ru(bpy)(CH_3CN)_2(dppcb)Os(bpy)_2](PF_6)_4$ (**9**)

Compound	Excitation band maxima, nm		Emission band maxima, nm	
	298 K[b]	77 K[c]	298 K[b]	77 K[c]
2	530	500	550[a]	560[a]
3	465	465	600	529
4		430		521
7	275	270	385[a]	455[a]
8	290	260	400[a]	480[a]
9	300	300	595	565

[a] The emission band maxima at 298 K and 77 K, respectively, stem from different states, where the ^{3}MLCT emissions are very strong at 77 K and therefore dominate the emission bands at 77 K. These ^{3}MLCT emissions show a dramatically reduced intensity at 298 K in the case of **2** and completely disappear at 298 K in the cases **7** and **8**. Therefore, emissions from different states are now detectable at 298 K. [b] In degassed spectrograde CH_3CN. [c] **2**–**4**: in a 4:1:2 (v/v, degassed spectrograde quality) $EtOH/MeOH/CH_3CN$ mixture; **7**–**9**: in a 10:1:5 (v/v, degassed spectrograde quality) $EtOH/glycerol/CH_3CN$ mixture.

Details of the electrochemical measurements:

Electrochemical measurements were made with an EG&G PAR Model 264A voltameter. Cyclic voltammetry was carried out with a 2-mm platinum-disk working electrode, a platinum-wire counter electrode and a Ag/AgCl pseudoreference electrode. 0.05 M Me_4NClO_4 was used as the electrolyte. Potentials are quoted relative to an SSCE at a scan rate of 100 mV s^{-1} and in degassed MeCN ($4 \cdot 10^{-3}$ M) of purissimum grade quality at room temperature.

The electrochemical behavior of compounds **2**–**4** and **9** is given in the experimental section. Also the electrochemical data for the complexes **1** and **5**/**6** are known and have been already published.[2b,5a] In the cases of the species **7** and **8** it was not possible to obtain enough pure substance in order to prevent irreversible behavior in the electrochemical measurements.

The $Ru^{II/III}$ couples related to the $[Ru(bpy)_2]^{2+}$ moieties in **1**–**6** occur in the range from +1.10 to +1.28 V being in line with earlier results.[5b,12a] The $Os^{II/III}$ couples related to the $[Os(bpy)_2]^{2+}$ moieties are shifted from +0.92 V in **5**/**6** to +1.51 V in **9**, where this range is also in agreement with related compounds.[4b] The different steps of bpy reductions occur in the range from –1.13 to –2.17 V for the complexes **1**–**6** and **9** being also typical of this class of compounds.[5b,27]

However, the most important issue, when thinking about the use of photosensitizers to operate in energy conversion cycles, is the feasibility of highly reactive metal sites in the cases of **2** and **3**. Thus, in **2** the $Pt^{II/0}$ couple occurs at –0.33 V and in **3** the $Pd^{II/0}$ couple at –0.14 V.[4b] Since in both cases ^{3}MLCT states are populated, where bpy ligands are reduced, it becomes clear that also highly reactive Pt^0 or Pd^0 sites are thermodynamically possible. Interestingly, no analogous $Ni^{II/0}$ couple has been observed for **4**, indicating that it is by no means easy to replace noble metals with inexpensive metals.